Extrastriatal dopamine D2/3 receptor binding, functional connectivity, and autism socio-communicational deficits: a PET and fMRI study

Title:

Extrastriatal dopamine D2/3 receptor binding, functional connectivity, and autism socio-communicational deficits: a PET and fMRI study

Authors

Chihiro Murayama, MD[1], Toshiki Iwabuchi, PhD[2,3], Yasuhiko Kato, MD, PhD[1], Masamichi Yokokura, MD[1,2], PhD, Taeko Harada, PhD[2,3], Takafumi Goto, MD[1], Taishi Tamayama, MD[1], Yosuke Kameno, MD, PhD[1], Tomoyasu Wakuda, MD, PhD[1], Hitoshi Kuwabara, MD, PhD[1,2], Atsushi Senju, PhD[2,3,4], Sadahiko Nishizawa, MD, PhD[5], Yasuomi Ouchi, MD, PhD[6,7], Hidenori Yamasue, MD, PhD[1,2]*

Affiliations

[1] Department of Psychiatry, Hamamatsu University School of Medicine, Hamamatsu, Japan.

[2] United Graduate School of Child Development, Hamamatsu University School of Medicine, Hamamatsu, Japan

[3] Research Center for Child Mental Development, Hamamatsu University School of Medicine, Hamamatsu, Japan

[4] Centre for Brain and Cognitive Development, Birkbeck, University of London, London, United Kingdom

[5] Hamamatsu Medical Imaging Center, Hamamatsu Medical Photonics Foundation, Hamamatsu, Japan.

[6] Global Strategic Challenge Center, Hamamatsu Photonics K.K., Hamamatsu, Japan.

[7] Department of Biofunctional Imaging, Hamamatsu University School of Medicine, Hamamatsu, Japan.

*Corresponding Author: H. Yamasue

Department of Psychiatry, Hamamatsu University School of Medicine, 1-20-1 Handayama, Higashiku, Hamamatsu City 431-3192, Japan

Phone: +81-53-435-2295; Fax: +81-53-435-3621; E-mail: yamasue@hama-med.ac.jp

Running title: Lower extrastriatal D2/3R binding in autism

Abstract

The social motivation hypothesis of autism proposes that social communication symptoms in autism spectrum disorder (ASD) stem from atypical social attention and reward networks, where dopamine acts as a crucial mediator. However, despite evidence indicating that individuals with ASD show atypical activation in extrastriatal regions while processing reward and social stimuli, no previous studies have measured extrastriatal dopamine D2/3 receptor (D2/3R) availability in ASD. Here, we investigated extrastriatal D2/3R availability in individuals with ASD and its association with ASD social communication symptoms using positron emission tomography (PET). Moreover, we employed a whole-brain multivariate pattern analysis of resting-state functional magnetic resonance imaging (fMRI) to identify regions where functional connectivity atypically correlates with D2/3R availability depending on ASD diagnosis. Twenty-two psychotropic-free males with ASD and 24 age- and intelligence quotient-matched typically developing males underwent [^{11}C]FLB457 PET, fMRI, and clinical symptom assessment. Participants with ASD showed lower D2/3R availability throughout the D2/3R-rich extrastriatal regions of the dopaminergic pathways. Among these, the posterior region of the thalamus, which primarily comprises the pulvinar, displayed the largest effect size for the lower D2/3R availability, which correlated with a higher score on the Social Affect domain of the Autism Diagnostic Observation Schedule-2 in

participants with ASD. Moreover, lower D2/3R availability was correlated with lower

functional connectivity of the thalamus-superior temporal sulcus and cerebellum-medial

occipital cortex, specifically in individuals with ASD. The current findings provide novel

molecular evidence for the social motivation theory of autism and offer a novel therapeutic

target.

Introduction

Atypical social communication, as well as stereotyped behavior and restricted interests, constitute the core symptoms of autism spectrum disorder (ASD)(1). Although the neurobiological mechanisms of these core symptoms remain largely unknown, the social motivation hypothesis of autism proposes that the atypical development of social communication stems from atypical social attention and reward networks that support social motivation (2). Given that dopamine acts as a crucial mediator for both social attention and reward networks (3, 4), dysfunctional dopaminergic systems are likely implicated in the atypical social communication observed in individuals with ASD. Previous positron emission tomography (PET) studies in ASD have shown higher orbitofrontal dopamine transporter (DAT) binding (5) and correlations between striatal and extrastriatal dopamine D1 receptor binding and clinical characteristics of ASD (6). Although a PET study using [11C]raclopride revealed higher striatal dopamine D2/3 receptor (D2/3R) availability in an ASD group following a reward task (7), no previous studies have measured extrastriatal D2/3R availability in individuals with ASD despite evidence demonstrating atypical activation in extrastriatal regions (e.g., the anterior cingulate cortex [ACC], thalamus, and amygdala) during the processing of reward and social stimuli, (8-10).

As for D2/3R, several lines of evidence have supported an association with social interaction and communication: DRD2 polymorphisms, which are related to D2R expression (11) or ASD diagnosis (12), are associated with friendship formation (13, 14), initiating joint attention skills (15), and core socio-communicational symptoms of ASD (12). In primates, administration of a D2R antagonist decreases the duration of gazing toward social images (4), which suggests that D2R plays a role in the processing of visual social attention, whereas administration of D3R antagonists increases social interaction and reduces aggression in mice (16, 17).

Atypical brain connectivity has been implicated in ASD socio-communicational symptoms (18, 19). Although its molecular mechanisms remain unclear, the alteration of D2/3R expression is a potential candidate because brain connectivity changes in proportion to changes in D2/3R expression. In mice, D2R overexpression decreases dendric spine numbers and entorhinal cortex-hippocampal connectivity (20). In humans, pharmacological functional magnetic resonance imaging (fMRI) studies have demonstrated that the administration of D2/3R antagonists modulates intrinsic functional connectivity in healthy adults (21-24). Moreover, multimodal PET and fMRI studies have revealed associations between D2/3R availability and widespread functional connectivity networks (25-29).

The purpose of the present PET and fMRI combination study using [^{11}C]FLB457, a radioligand for extrastriatal D2/3R, was to investigate 1) whether extrastriatal D2/3R in adult males with ASD are different from those in typically developing (TD) individuals, 2) whether atypical extrastriatal D2/3R correlate with ASD socio-communicational symptoms, and 3) whether atypical extrastriatal D2/3R are associated with atypical brain functional connectivity. Considering the association between a genetically determined decrease in D2R expression and an increased probability of ASD diagnosis and symptoms (11, 12, 15, 30), we hypothesized that compared with TD individuals, adult males with ASD would have lower D2/3R, and that this would be correlated with more pronounced socio-communicational symptoms. Furthermore, we hypothesized that associations between D2/3R expression and atypical functional connectivity in ASD would be predicted by the influence of D2/3R expression on brain connectivity (20, 24).

Materials and Methods

Participants

The study protocol was approved by the Ethics Committee of the Hamamatsu University School of Medicine. All participants provided written informed consent before joining the

study. Individuals with ASD were recruited from the Hamamatsu University School of

Medicine Hospital. The inclusion criteria for the ASD group were as follows: 1) ≥ 18 years of

age; 2) male; 3) diagnosed with ASD according to the Diagnostic and Statistical Manual-

Revision 5 (1); 4) diagnosis confirmed according to the Autism Diagnostic Interview-Revised

(ADI-R) (31) and Autism Diagnostic Observation Schedule-2 (ADOS-2) (32) by a

psychologist certified for research uses (T.H.); 5) full-scale intelligence quotient (IQ) > 70 on

the Wechsler Adult Intelligence Scale-Third Edition (33). Furthermore, to minimize the

potential confounding effects, we recruited individuals without any psychiatric comorbidities

according to the Structured Clinical Interview for DSM-5 Research Version (34). Age- and

IQ-matched TD males were recruited through public advertisements. All participants

completed the Autism-Spectrum Quotient (35). Socioeconomic status (SES) was assessed in

participants and their parents using the Hollingshead scale (36). The exclusion criteria for all

participants were 1) the presence of gross abnormalities in T2 or FLAIR head MRI, 2) the

presence of a major medical illness, and 3) a history of having taken psychotropic drugs

within the past 4 weeks. TD participants with any current or previous neurological or

psychiatric disorders were also excluded.

PET data acquisition

A high-resolution brain PET scanner (SHR12000, Hamamatsu Photonics K.K., Hamamatsu, Japan) was used to acquire 47 tomographic images simultaneously (37, 38). All participants underwent a PET scan with [^{11}C]FLB457 PET tracer to measure extrastriatal D2/3R. After back-projection and filtering (Hanning filter, cut-off frequency of 0.2 cycles per pixel), the image resolution was $2.9 \times 2.9 \times 3.4$ mm full-width half-maximum. The voxel of each reconstructed image measured $1.3 \times 1.3 \times 3.4$ mm. A thermoplastic face mask was used to prevent the participant's head from moving during the scan. A bolus of [^{11}C]FLB457 (2 MBq/kg) was injected intravenously via a cannula for 10 seconds. The cannula was then immediately flushed with 20 ml of saline. After the intravenous injection of the tracer, dynamic PET scans with 33 frames (time frames: 6×10, 3×20, 6×60, 4×180, and 14×300 s) were performed over 90 min.

The binding potential (BP_{ND}) parametric images of [^{11}C]FLB457 were estimated using a simplified reference tissue model by applying a normalized time activity curve based on the cerebellar cortex of each participant (39). All BP_{ND} parametric images were generated using PMOD 3.8 software (PMOD Technologies, Ltd., Switzerland). The affinity of [^{11}C]FLB to the D2 receptor in the striatum is too high to calculate the binding potential quantitatively,

8

so this tracer does not allow evaluation of the D2 receptor in the striatum but in the thalamus instead (40).

MRI data acquisition

A 3-Tesla magnetic resonance scanner (Ingenia, Royal Philips, Eindhoven, Netherland) was used to acquire T1-weighted images to normalize the functional data and establish regions of interest (ROIs) and T2*-weighted gradient-echo echo-planar images for resting-state fMRI. The detailed acquisition parameters and procedures are described in the Supplementary Methods.

ROI analysis

ROIs were manually traced in individual MRI spaces, blinded to group status, in the following 10 extrastriatal brain regions that have relatively abundant distributions of D2/3R (41) and belong to the major components of the dopaminergic pathways (42): the ventral tegmental area, substantia nigra, amygdala, dorsal and rostral anterior cingulate cortices (dACC/rACC), and five thalamic subregions (Supplementary Figures 1−3). To enhance the local sensitivity of the ROI analysis, the ACC and thalamus were divided into subregions.

However, the amygdala was not subdivided because of the insufficient spatial resolution of

PET images for segmenting amygdala subnuclei. Warping of the atlases in the process of

transformation to the individual PET images via automated ROI creation may lead to mis-

delineation, although the reference region can be defined separately for each individual before

spatial normalization (43). In contrast, hand-drawn ROI delineation is more exact but relies

on subjective choices. To minimize between-study variance resulting from operator-

dependent choices, a single operator (C.M.) who was blind to group status delineated all the

ROIs for all participants in this study. We performed subdivisions of the ACC and thalamus

using anatomical landmarks or percentage-based parameters to reduce subjectivity. In the

thalamus, $[^{11}C]$FLB457 signals had a highly heterogeneous distribution (44), which is

consistent with the distinct dopamine innervation patterns of the thalamic nuclei (45, 46). In

fact, dividing the thalamus into five subregions increased the sensitivity for detecting

differences between patients with specific psychiatric disorders and controls (47, 48). The

detailed procedures for dividing the ACC into two subregions and the thalamus into five

subregions are described elsewhere (48-51)(see also Supplementary Methods and

Supplementary Figures 2 & 3). We transferred each ROI onto the corresponding BP_{ND}

parametric image and obtained a BP_{ND} value for each ROI. The creation of the parametric

BP_{ND} images and subsequent kinetic analysis was performed in individual PET spaces after

delineating the ROIs in individual MRI spaces and transferring them to the individual PET

spaces.

Statistical analyses for demographic, clinical, and PET data

All statistical analyses for demographic, clinical, and PET data were performed using SPSS

version 25 (IBM, Armonk, NY). Demographic and clinical variables were compared between

the ASD and TD groups using independent-samples t-tests. The threshold for statistical

significance was $p < 0.05$.

To compare BP_{ND} values between the ASD and TD groups, we used an analysis of

variance (ANOVA), with diagnosis (i.e., ASD/TD) as a between-subjects factor and ROI as a

within-subjects factor. The statistical threshold for the ANOVA was $p < 0.05$. For significant

interactions between diagnosis and ROI, regional contrasts in the 10 ROIs were investigated

using post hoc t-tests with Bonferroni correction for multiple comparisons.

To investigate the clinical correlates of differential BP_{ND} values, we correlated BP_{ND}

values with ADOS-2 scores. In addition to the reciprocity, communication, and repetitive and

restricted behavior scores of the ADOS-2, we calculated the total score for the Social Affect

domain of the ADOS-2 algorithm (SA-revised)(52), which consists of communication and

reciprocity scores, was calculated to examine the correlation between D2/3R availability and

socio-communication symptoms. According to the results from the group comparison of BP_{ND}

values, Pearson's correlation analyses were conducted between the BP_{ND} values of the 10

ROIs and the four ADOS-2 scores using the Bonferroni correction for multiple comparisons

at a statistical threshold of $p < 0.00125$ (= 0.05/40 correlations).

Resting-state fMRI data preprocessing and analysis

The CONN toolbox version 20.b (53) and SPM12 (http://www.fil.ion.ucl.ac.uk/spm/) were

used to analyze the resting-state fMRI data (see Supplementary Methods for detailed

descriptions of the fMRI data preprocessing and denoising).

An important implication from previous studies is that altered D2/3R availability in a

specific region influences widespread functional networks that are outside of that region (25,

28, 29). Thus, we employed multivariate pattern analysis (MVPA) to explore regions where

whole-brain functional connectivity patterns were differently modified between diagnostic

groups based on D2/3R availability in a voxel-by-voxel manner (see Supplementary Methods

for details).

MVPA was performed to identify regions where whole-brain functional connectivity

showed an interaction between diagnosis and D2/3R availability. We used [11C]FLB457 BP_{ND}

values averaged across the 10 ROIs in the statistical model based on the result (i.e. a significant main effect of diagnosis on $[^{11}C]FLB457$ BP_{ND} values without an interaction between diagnosis and ROI, see Results). After identifying significant clusters using MVPA, we performed a post hoc seed-to-voxel analysis using these clusters as seed regions. This analysis further tested the interaction between D2/3R availability and ASD diagnosis on the functional connectivity between these seed regions and the rest of the brain. For clusters identified by the post hoc analyses, we calculated Pearson's correlation coefficients between functional connectivity and ADOS-2 scores with Bonferroni correction for multiple comparisons.

Results

Participant demographic information

Participants were recruited from October 31, 2017, to April 1, 2020. Twenty-three psychotropic-free individuals with ASD and 24 age-, sex- and IQ-matched TD individuals were recruited (Table 1). No participants in this study were taking medication, and none had a current psychiatric comorbidity. The PET data from one participant with ASD were excluded. This participant reported neck pain during the PET scan and was not able to remain

motionless, so we stopped scanning in the middle of the PET scan. The individuals with ASD

showed significantly higher Autism-Spectrum Quotient ($p < 0.001$) and self-SES (indicating

lower status, $p < 0.001$) scores compared with the TD individuals (Table 1), whereas no

significant group difference was found in age, height, body mass index, or parental SES, or

full, verbal, or performance IQ.

Group differences in [11C]FLB457 BP$_{ND}$ values between the ASD and TD groups

Representative [11C]FLB457 PET images are shown in Supplementary Figure 4. The

ANOVA revealed significant main effects of diagnosis ($F_{9,440} = 22.905$, $p < 0.001$) and ROI

($F_{9,440} = 117.964$, $p < 0.001$). However, there was no significant interaction between diagnosis

and ROI ($F_{9,440} = 0.603$, $p = 0.794$). The significant main effect of diagnosis and the mean

values of each ROI in each diagnostic group (Table 2) indicated lower [11C]FLB457 BP$_{ND}$

values, averaged across ROIs, in individuals with ASD compared with those in the TD group.

Although the non-significant interaction between diagnosis and ROI indicated that there was

no significant difference in the degree of atypicality between the ROIs, the effect sizes of the

ROIs were estimated to evaluate the atypicality among the ROIs. Among the 10 ROIs, the

effect size for the posterior region of the thalamus (Cohen's d = 0.95) was large, and the

central lateral (Cohen's d = 0.61) and anterior medial regions (Cohen's d = 0.59) of the

thalamus, amygdala (Cohen's d = 0.65), and dACC (Cohen's d = 0.53) had medium effect

sizes (Table 2; Figure 1)

Correlations between [^{11}C]FLB457 BP$_{ND}$ values and ADOS-2 scores

Although we excluded one individual with ASD from the correlational analyses because they

refused to take the ADOS-2, the main effect of diagnosis on BPND values of [11C]FLB45

was preserved in the ASD (N = 21) and TD (N = 24) groups (F9,430 = 23.018, p < 0.001). In

individuals with ASD, we found a significant negative correlation between the [11C]FLB457

BPND value in the posterior region of the thalamus and the ADOS-2 SA-revised score (r = −

0.68; uncorrected p = 0.00074; Bonferroni-corrected p < 0.05; Figure 2). The [11C]FLB457

BPND value in the posterior thalamus was not significantly correlated with the other ADOS

scores. None of the other ROIs showed significant correlations between [11C]FLB45 BPND

values and ADOS scores (Supplementary Figure 5).

Results of the MVPA of resting-state fMRI data

Because the main ANOVA revealed a significant effect of diagnosis on [^{11}C]FLB457 BP$_{ND}$

values without an interaction between diagnosis and ROI, we used [^{11}C]FLB457 BP$_{ND}$ values

averaged across all 10 ROIs as an independent variable in the MVPA. Whole-brain MVPA

revealed significant clusters in the bilateral thalamus (Figure 3A, [−8, −18, 18], cluster size = 104) and the right cerebellum (Figure 3A, [28, −60, −24], cluster size = 94). This suggests that whole-brain functional connectivity patterns from these two regions were differentially correlated with the D2/3R availability between the ASD and TD groups.

The post hoc analyses using the clusters of the thalamus and the right cerebellum as seeds showed that when the thalamus cluster was used as a seed, we found significant clusters lying along the bilateral superior temporal sulcus (STS). This suggests that D2/3R availability was associated with differential thalamus-STS functional connectivity between groups (Figure 3B and Table 3). The post hoc analysis of the right cerebellum seed revealed that the right postcentral gyrus and medial occipital cortex, which included the lingual gyrus and a large region of the cuneus, showed a significant diagnosis $\times$ D2/3R interaction (Figure 3B and Table 3). This suggested a significant group difference in the correlation between functional connectivity and the averaged [^{11}C]FLB457 BP_{ND} values. Within the ASD group, lower D2/3R availability was significantly associated with lower functional connectivity, except for cerebellar-postcentral connectivity, as shown by the post hoc analyses (Supplementary Figure 6). We also examined the correlations between ADOS-2 scores and functional connectivity; however, no significant correlations were found for either the thalamus or right cerebellum seed (Supplementary Table 1).

Discussion

To the best of our knowledge, this is the first study to evaluate extrastriatal D2/3R availability

in vivo in adult males with ASD. We found that D2/3R availability throughout the D2/3R-rich

extrastriatal regions of the dopaminergic pathways was lower in adult males with ASD than in

TD males. Among the extrastriatal regions, the posterior thalamus showed the largest effect

size for lower D2/3R availability, and this was correlated with socio-communication

difficulties in adult males with ASD. Moreover, the low D2/3R availability in the ASD group

was correlated with low functional connectivity between the thalamus and STS and between

the cerebellum and medial occipital cortex.

Consistent with our hypothesis, extrastriatal D2/3R availability was lower in adult

males with ASD than in TD individuals. Unlike in the striatal regions, extrastriatal

[11C]FLB457 was not sensitive to endogenous dopamine (54). Therefore, the lower D2/3R

availability in adult males with ASD was attributed, not to the increase in endogenous

dopamine, but rather, to the low receptor density. Our finding of low D2/3R density in adult

males with ASD is in line with a previous genetic study, which revealed that a polymorphism

in DRD2 associated with reduced D2 receptor expression increased the risk of developing

17

ASD (11, 30). This DRD2 polymorphism was also associated with lower initiation of joint attention in younger siblings of children with ASD (15), which suggests a link between low D2/3R density and social attention challenges in ASD. Furthermore, another polymorphism in DRD2, which also increased the likelihood of ASD diagnosis, was associated with social interaction and communication scores in the ADI-R (12). These studies support our finding of a correlation between low D2/3R density and socio-communicational challenges in ASD.

Although the interaction between ROI and ASD diagnosis was not statistically significant, the effect sizes for the thalamic subregions, amygdala, and dACC were relatively large among the D2/3R-rich extrastriatal regions. A previous meta-analysis showed that ASD individuals exhibit atypical fMRI activation in the thalamus, amygdala, and ACC during reward processing (8). Thus, our finding of low D2/3R density in these extrastriatal regions may be linked to dysfunctional reward circuitry in ASD, thus providing a molecular basis for the social motivation theory of autism. However, our finding is inconsistent with previous reports of increased D2/3R availability in ASD (7). Unlike in the present study, the increased D2/3R availability was detected in response to a reward task and only in striatal regions where D2/3R availability is sensitive to endogenous dopamine (54), suggesting that the striatal and extrastriatal regions influence D2/3R availability via distinct mechanisms.

Among the subregions of the thalamus, the posterior subregion, which primarily

comprises the pulvinar (Supplementary Figure 2), had the largest effect size for decreased D2/3R availability in ASD. This decrease was strongly correlated with the ADOS SA-revised score. The pulvinar, together with the superior colliculus and amygdala, is thought to form a subcortical pathway that mediates subconscious facial expression perception (55) and face-related preferences (56), which are closely related to visual social attention. The notion that atypical functioning of these subcortical pathways leads to social communication difficulties in individuals with ASD was proposed as the fast-track modulator model of ASD (57). Although the precise function of these subcortical pathways has been debated, the critical role of the pulvinar and amygdala in coordinating socio-affective processing has also been highlighted by other competing theories on the subcortical processing of social information (58). The social motivation theory of autism also posits that early-onset symptoms of social attention cause socio-communication difficulties in ASD (2). Indeed, atypical functioning of these subcortical structures has been demonstrated in fMRI studies, whereby ASD individuals exhibited atypical activation of these subcortical pathway components during emotional face processing (9, 10). Our finding that the decreased D2/3R density in the pulvinar was correlated with socio-communicational difficulties in ASD not only supports but also provides a molecular basis for the social motivation theory and demonstrates the crucial role of these subcortical structures in social functioning and ASD.

Adult males with ASD showed an atypical positive correlations between the averaged D2/3R availability in the extrastriatal regions and functional connectivity between the thalamus–STS, cerebellum–medial occipital cortex, and cerebellum–postcentral gyrus. Consistent with our findings, functional connectivity and diffusion tensor imaging tractography studies revealed atypical connectivity between several subregions of the thalamus, including the pulvinar, and the STS in individuals with ASD (59, 60). The STS is a key structures in the cortical social brain network and is involved in the visual analysis of social information conveyed by gaze direction, body movement, and other types of biological motions (61). Atypical activation of the STS during the processing of gaze shifts that convey intentions has been reported in individuals with ASD (62). Moreover, the fast-track modulator model of ASD proposes that the atypical activation and structural patterns of the cortical social brain network, including the STS, occur simultaneously with the atypical functioning of the subcortical pathways (56, 57).

The cuneus in the medial occipital cortex and postcentral gyrus are hub regions of the visual and somatosensory cortical networks, respectively, and are connected to the cerebellum in TD individuals (63). However, individuals with ASD display altered resting-state functional connectivity between the cerebellum and sensorimotor cortices, which included the cuneus and postcentral gyrus (64). In our study, TD individuals exhibited a negative

correlation between the averaged extrastriatal D2/3R availability and functional connectivity

between the thalamus–STS, cerebellum–cuneus, and cerebellum–postcentral gyrus, which is

consistent with an animal study showing that D2R overexpression reduces dendric spine

numbers and entorhinal cortex–hippocampal connectivity (20). In contrast, the atypical

positive correlations between the extrastriatal D2/3R availability and functional connectivity

observed in adult males with ASD may reflect a disruption in the typical role of D2R in the

development of brain connectivity networks. Taken together, our results illuminate the

molecular mechanism underlying atypical functional connectivity in ASD.

Presynaptic D2/3 receptor and DAT directly interact, and this complex modulates

synaptic dopamine levels (65). In the current study, we found lower D2/3 receptor binding in

men with ASD throughout the extrastriatal regions, while a previous study found higher DAT

binding in the orbitofrontal cortex of subjects with ASD (5). This relationship might be

explained by reduced DAT expression in limbic forebrain synaptosomes induced by D3

receptor stimulation (66), although the exact relationship between D2/3 receptor expression

and DAT expression remains largely unknown in ASD.

Our study has several limitations. First, participants in this study were all adult

Japanese males with high-functioning ASD without psychiatric comorbidities, and the

homogeneity of participants may have contributed to the detection of robust group differences

21

and correlations. However, this limits the generalization of our findings to other demographic groups. In addition, since we did not evaluate the subthreshold ADHD symptoms in the participants, we were not able to rule out the potential confounding effects of subthreshold ADHD symptoms on the current findings. Second, our thalamic subdivision methodology has several limitations. Because there was no intrathalamic marker that could be used as a consistent landmark to delineate the thalamic subregions, we applied approximate percentage-based divisions. Although this automated method is effective for reducing subjectivity and systematic bias when defining thalamic subregions in imaging data with a limited resolution, some participants may have thalamic nuclei that are not in proportion to the percentage-based parameters defined in this study. Although atlases that divide the thalamus on the basis of histological stains (e.g., Nissl, myelin, calcium-binding proteins, thenon-phosphorylated neurofilament protein and acetylcholinesterase) have been proposed (67), these staining patterns do not match the dopamine innervation pattern (46). Moreover, fine subdivisions in such atlases are beyond the limits of the spatial resolution of our PET scanner (i.e. 6.8 mm). Higher-resolution imaging will be required to delineate using an intrathalamic marker, which would improve the reliability of our approach. Finally, two participants in the TD group were habitual cigarette smokers. Considering that nicotine induces dopamine release and decreases D2/3R availability in extrastriatal regions (68), these two TD participants may have reduced

group differences. However, this influence is likely to be small, and the conclusions of this study did not change when analyses were performed without these habitual cigarette smokers.

In the current study, we found significantly lower extrastriatal D2/3R density in vivo in adult males with ASD. The effect size of the reduction was largest in the pulvinar, where D2/3R availability was correlated with socio-communicational difficulties in ASD. Moreover, D2/3R density in adult males with ASD was associated with atypical connectivity between the thalamus–STS, cerebellum–cuneus, and cerebellum–postcentral gyrus. These results not only support but also provide a molecular basis for the social motivation theory and the fast-track modulator model of ASD.

Acknowledgments

Conflict of Interest

The authors declare no conflicts of interest.

Authors' contributions

H.Y. had full access to all the data in the study and takes responsibility for the integrity of the

data and the accuracy of the data analysis. Study concept and design: M.Y., Y.O., H.Y..

Acquisition, analysis, or interpretation of data: C.M. , Ya.K., M.Y., T.I., T.H., T.G., T.T.,

Yo.K., T.W., H.K., S.B., A.S., Y.O., H.Y.. Drafting of the manuscript: C.M., T.I., H.Y.. Critical

revision of the manuscript for important intellectual content: T.I., M.Y., T.H., T.G., T.T.,

References

1. American Psychiatric Association. Diagnostic and Statistical Manual of Mental Disorders. 5th ed, text revision. Washington DC: *American Psychiatric Association Publishing*; 2013.

2. Chevallier C, Kohls G, Troiani V, Brodkin ES, Schultz RT. The social motivation theory of autism. *Trends Cogn Sci.* 2012;**16**(4):231-9.

3. Hung LW, Neuner S, Polepalli JS, Beier KT, Wright M, Walsh JJ, et al. Gating of social reward by oxytocin in the ventral tegmental area. *Science*. 2017;**357**(6358):1406-11.

4. Yamaguchi Y, Atsumi T, Poirot R, Lee YA, Kato A, Goto Y. Dopamine-dependent visual attention preference to social stimuli in nonhuman primates. *Psychopharmacology*. 2017;**234**(7):1113-20.

5. Nakamura K, Sekine Y, Ouchi Y, Tsujii M, Yoshikawa E, Futatsubashi M, et al. Brain serotonin and dopamine transporter bindings in adults with high-functioning autism. *Arch Gen Psychiatry*. 2010;**67**(1):59-68.

6. Kubota M, Fujino J, Tei S, Takahata K, Matsuoka K, Tagai K, et al. Binding of Dopamine D1 Receptor and Noradrenaline Transporter in Individuals with Autism Spectrum Disorder: A PET Study. *Cereb Cortex*. 2020;**30**(12):6458-68.

7. Zurcher NR, Walsh EC, Phillips RD, Cernasov PM, Tseng CJ, Dharanikota A, et al. A simultaneous [(11)C]raclopride positron emission tomography and functional magnetic resonance imaging investigation of striatal dopamine binding in autism. *Transl Psychiatry*. 2021;**11**(1):33.

8. Clements CC, Zoltowski AR, Yankowitz LD, Yerys BE, Schultz RT, Herrington JD. Evaluation of the Social Motivation Hypothesis of Autism: A Systematic Review and Meta-analysis. *JAMA Psychiatry*. 2018;**75**(8):797-808.

9. Kleinhans NM, Richards T, Johnson LC, Weaver KE, Greenson J, Dawson G, et al. fMRI evidence of neural abnormalities in the subcortical face processing system in ASD. *Neuroimage*. 2011;**54**(1):697-704.

10. Hadjikhani N, Asberg Johnels J, Zurcher NR, Lassalle A, Guillon Q, Hippolyte L, et al. Look me in the eyes: constraining gaze in the eye-region provokes abnormally high subcortical activation in autism. *Sci Rep*. 2017;**7**(1):3163.

11. Thompson J, Thomas N, Singleton A, Piggott M, Lloyd S, Perry EK, et al. D2 dopamine receptor gene (DRD2) Taq1 A polymorphism: reduced dopamine D2 receptor binding in the human striatum associated with the A1 allele. *Pharmacogenetics*. 1997;**7**(6):479-84.

12. Hettinger JA, Liu X, Hudson ML, Lee A, Cohen IL, Michaelis RC, et al. DRD2 and PPP1R1B (DARPP-32) polymorphisms independently confer increased risk for autism

spectrum disorders and additively predict affected status in male-only affected sib-pair families. *Behav Brain Funct*. 2012;**8**:19.

13. Boardman JD, Domingue BW, Fletcher JM. How social and genetic factors predict friendship networks. *Proc Natl Acad Sci USA*. 2012;**109**(43):17377-81.

14. Fowler JH, Settle JE, Christakis NA. Correlated genotypes in friendship networks. *Proc Natl Acad Sci USA*. 2011;**108**(5):1993-7.

15. Gangi DN, Messinger DS, Martin ER, Cuccaro ML. Dopaminergic variants in siblings at high risk for autism: Associations with initiating joint attention. *Autism Res*. 2016;**9**(11):1142-50.

16. Rodríguez-Arias M, Felip CM, Broseta I, Miñarro J. The dopamine D3 antagonist U-99194A maleate increases social behaviors of isolation-induced aggressive male mice. *Psychopharmacology*. 1999;**144**(1):90-4.

17. Cosi C, Martel JC, Auclair AL, Collo G, Cavalleri L, Heusler P, et al. Pharmacology profile of F17464, a dopamine D(3) receptor preferential antagonist. *Eur J Pharmacol*. 2021;**890**:173635.

18. Hull JV, Dokovna LB, Jacokes ZJ, Torgerson CM, Irimia A, Van Horn JD. Resting-State Functional Connectivity in Autism Spectrum Disorders: A Review. *Front Psychiatry*. 2016;**7**:205.

19. Kana RK, Uddin LQ, Kenet T, Chugani D, Muller RA. Brain connectivity in autism. *Front Hum Neurosci*. 2014;**8**:349.

20. Jia JM, Zhao J, Hu Z, Lindberg D, Li Z. Age-dependent regulation of synaptic connections by dopamine D2 receptors. *Nat Neurosci*. 2013;**16**(11):1627-36.

21. Cole DM, Beckmann CF, Oei NY, Both S, van Gerven JM, Rombouts SA. Differential and distributed effects of dopamine neuromodulations on resting-state network connectivity. *Neuroimage*. 2013;**78**:59-67.

22. Cole DM, Oei NY, Soeter RP, Both S, van Gerven JM, Rombouts SA, et al. Dopamine-dependent architecture of cortico-subcortical network connectivity. *Cereb Cortex*. 2013;**23**(7):1509-16.

23. Grimm O, Kopfer V, Kupper-Tetzel L, Deppert V, Kuhn M, de Greck M, et al. Amisulpride and l-DOPA modulate subcortical brain nuclei connectivity in resting-state pharmacologic magnetic resonance imaging. *Hum Brain Mapp*. 2020;**41**(7):1806-18.

24. Kahnt T, Tobler PN. Dopamine Modulates the Functional Organization of the Orbitofrontal Cortex. *J Neurosci*. 2017;**37**(6):1493-504.

25. Cole DM, Beckmann CF, Searle GE, Plisson C, Tziortzi AC, Nichols TE, et al. Orbitofrontal connectivity with resting-state networks is associated with midbrain dopamine D3 receptor availability. *Cereb Cortex*. 2012;**22**(12):2784-93.

26. Yamada M, Uddin LQ, Takahashi H, Kimura Y, Takahata K, Kousa R, et al. Superiority illusion arises from resting-state brain networks modulated by dopamine. *Proc Natl Acad Sci USA*. 2013;**110**(11):4363-7.

27. Nyberg L, Karalija N, Salami A, Andersson M, Wahlin A, Kaboovand N, et al. Dopamine D2 receptor availability is linked to hippocampal-caudate functional connectivity and episodic memory. *Proc Natl Acad Sci USA*. 2016;**113**(28):7918-23.

28. Nagano-Saito A, Lissemore JI, Gravel P, Leyton M, Carbonell F, Benkelfat C. Posterior dopamine D2/3 receptors and brain network functional connectivity. *Synapse*. 2017;**71**(11).

29. Nour MM, Dahoun T, McCutcheon RA, Adams RA, Wall MB, Howes OD. Task-induced functional brain connectivity mediates the relationship between striatal D2/3 receptors and working memory. *Elife*. 2019;**8**.

30. Salem AM, Ismail S, Zarouk WA, Abdul Baky O, Sayed AA, Abd El-Hamid S, et al. Genetic variants of neurotransmitter-related genes and miRNAs in Egyptian autistic patients. *Scientific World Journal*. 2013;**2013**:670621.

31. Lord C, Rutter M, Le Couteur A. Autism Diagnostic Interview-Revised: a revised version of a diagnostic interview for caregivers of individuals with possible pervasive developmental disorders. *J Autism Dev Disord*. 1994;**24**(5):659-85.

32. Lord C, Rutter M, Goode S, Heemsbergen J, Jordan H, Mawhood L, et al. Austism diagnostic observation schedule: A standardized observation of communicative and social behavior. *J Autism Dev Disord*. 1989;**19**(2):185-212.

33. Wechsler D. The psychometric tradition: Developing the Wechsler Adult Intelligence Scale. *Contemporary Educational Psychology*. 1981.

34. First MB, Williams JB, Karg RS, Spitzer RL, eds. Structured clinical interview for DSM-5—Research version. Arlington, VA: American Psychiatric Association; 2015:1-94.

35. Baron-Cohen S, Wheelwright S, Skinner R, Martin J, Clubley E. The autism-spectrum quotient (AQ): evidence from Asperger syndrome/high-functioning autism, males and females, scientists and mathematicians. *J Autism Dev Disord*. 2001;**31**(1):5-17.

36. Hollingshead AB. Two factor index of social position. *New Haven*. Yale University. 1957.

37. Watanabe M, Shimizu K, Omura T, Takahashi M, Kosugi T, Yoshikawa E, et al. A new high-resolution PET scanner dedicated to brain research. *IEEE Transactions on Nuclear Science*. 2002;**49**(3):634-9.

38. Terada T, Obi T, Bunai T, Matsudaira T, Yoshikawa E, Ando I, et al. In vivo mitochondrial and glycolytic impairments in patients with Alzheimer disease. *Neurology*. 2020;**94**(15):e1592-e604.

39. Lammertsma AA, Hume SP. Simplified reference tissue model for PET receptor studies. *Neuroimage*. 1996;**4**(3 Pt 1):153-8.

40. Ito H, Takahashi H, Arakawa R, Takano H, Suhara T. Normal database of dopaminergic neurotransmission system in human brain measured by positron emission tomography. *Neuroimage*. 2008;**39**(2):555-65.

41. Ayano G. Dopamine: Receptors, Functions, Synthesis, Pathways, Locations and Mental Disorders: Review of Literatures. *J Ment Disord Treat*. 2016;**2**(2).

42. Dichter GS, Damiano CA, Allen JA. Reward circuitry dysfunction in psychiatric and neurodevelopmental disorders and genetic syndromes: animal models and clinical findings. *J Neurodev Disord*. 2012;**4**(1):19.

43. Karjalainen T, Tuisku J, Santavirta S, Kantonen T, Bucci M, Tuominen L. Magia: Robust Automated Image Processing and Kinetic Modeling Toolbox for PET Neuroinformatics. *Front Neuroinform.* 2020;**14**:3.

44. Okubo Y, Olsson H, Ito H, Lofti M, Suhara T, Halldin C, et al. PET mapping of extrastriatal D2-like dopamine receptors in the human brain using an anatomic standardization technique and [11C]FLB 457. *Neuroimage*. 1999;**10**(6):666-74.

45. Sanchez-Gonzalez MA, Garcia-Cabezas MA, Rico B, Cavada C. The primate thalamus is a key target for brain dopamine. *J Neurosci*. 2005;**25**(26):6076-83.

46. Garcia-Cabezas MA, Rico B, Sanchez-Gonzalez MA, Cavada C. Distribution of the dopamine innervation in the macaque and human thalamus. *Neuroimage*. 2007;**34**(3):965-84.

47. Suhara T, Okubo Y, Yasuno F, Sudo Y, Inoue M, Ichimiya T, et al. Decreased dopamine D2 receptor binding in the anterior cingulate cortex in schizophrenia. *Arch Gen Psychiatry*. 2002;**59**(1):25-30.

48. Yasuno F, Suhara T, Okubo Y, Sudo Y, Inoue M, Ichimiya T, et al. Low dopamine d(2) receptor binding in subregions of the thalamus in schizophrenia. *Am J Psychiatry*. 2004;**161**(6):1016-22.

49. Gilbert AR, Rosenberg DR, Harenski K, Spencer S, Sweeney JA, Keshavan MS. Thalamic volumes in patients with first-episode schizophrenia. *Am J Psychiatry*. 2001;**158**(4):618-24.

50. Fornito A, Whittle S, Wood SJ, Velakoulis D, Pantelis C, Yücel M. The influence of sulcal variability on morphometry of the human anterior cingulate and paracingulate cortex. *Neuroimage*. 2006;**33**(3):843-54.

51. McCormick LM, Ziebell S, Nopoulos P, Cassell M, Andreasen NC, Brumm M. Anterior cingulate cortex: an MRI-based parcellation method. *Neuroimage*. 2006;**32**(3):1167-75.

52. Hus V, Lord C. The autism diagnostic observation schedule, module 4: revised algorithm and standardized severity scores. *J Autism Dev Disord*. 2014;**44**(8):1996-2012.

53. Whitfield-Gabrieli S, Nieto-Castanon A. Conn: a functional connectivity toolbox for correlated and anticorrelated brain networks. *Brain Connect*. 2012;**2**(3):125-41.

54. Okauchi T, Suhara T, Maeda J, Kawabe K, Obayashi S, Suzuki K. Effect of endogenous dopamine on extrastriatal [^{11}C]FLB 457 binding measured by PET. *Synapse*. 2001;**41**(2):87-95.

55. Ward R, Calder AJ, Parker M, Arend I. Emotion recognition following human pulvinar damage. *Neuropsychologia*. 2007;**45**(8):1973-8.

56. Johnson MH. Subcortical face processing. *Nat Rev Neurosci*. 2005;**6**(10):766-74.

57. Senju A, Johnson MH. Atypical eye contact in autism: models, mechanisms and development. *Neurosci Biobehav Rev*. 2009;**33**(8):1204-14.

58. Pessoa L, Adolphs R. Emotion processing and the amygdala: from a 'low road' to 'many roads' of evaluating biological significance. *Nat Rev Neurosci*. 2010;**11**(11):773-83.

59. Nair A, Treiber JM, Shukla DK, Shih P, Muller RA. Impaired thalamocortical connectivity in autism spectrum disorder: a study of functional and anatomical connectivity. *Brain*. 2013;**136**(Pt 6):1942-55.

60. Woodward ND, Giraldo-Chica M, Rogers B, Cascio CJ. Thalamocortical dysconnectivity in autism spectrum disorder: An analysis of the Autism Brain Imaging Data Exchange. *Biol Psychiatry Cogn Neurosci Neuroimaging*. 2017;**2**(1):76-84.

61. Allison T, Puce A, McCarthy G. Social perception from visual cues: role of the STS region. *Trends Cogn Sci*. 2000;**4**(7):267-78.

62. Pelphrey KA, Morris JP, McCarthy G. Neural basis of eye gaze processing deficits in autism. *Brain*. 2005;**128**(Pt 5):1038-48.

63. Tomasi D, Volkow ND. Association between functional connectivity hubs and brain networks. *Cereb Cortex*. 2011;**21**(9):2003-13.

64. Khan AJ, Nair A, Keown CL, Datko MC, Lincoln AJ, Muller RA. Cerebro-cerebellar Resting-State Functional Connectivity in Children and Adolescents with Autism Spectrum Disorder. *Biol Psychiatry*. 2015;**78**(9):625-34.

65. Lee FJ, Pei L, Moszczynska A, Vukusic B, Fletcher PJ, Liu F. Dopamine transporter cell surface localization facilitated by a direct interaction with the dopamine D2 receptor. *EMBO J*. 2007;**26**(8):2127-36.

66. Chang PK, Chien KY, Chen JC. Dopamine transporter is downregulated and its association with chaperone protein Hsc70 is enhanced by activation of dopamine D(3) receptor. *Brain Res Bull*. 2020;**165**:263-71.

67. Krauth A, Blanc R, Poveda A, Jeanmonod D, Morel A, Székely G. A mean three-dimensional atlas of the human thalamus: generation from multiple histological data. *Neuroimage* 2010;**49**(3):2053-62.

68. Wing VC, Payer DE, Houle S, George TP, Boileau I. Measuring cigarette smoking-induced cortical dopamine release: A [(1)(1)C]FLB-457 PET study. *Neuropsychopharmacology*. 2015;**40**(6):1417-27.

Figure legends

Figure 1. [¹¹C]FLB-457 binding potential (BP$_{ND}$) values of all 10 regions of interest in autism spectrum disorder (ASD) and typically developing (TD) individuals

Plots represent regional [¹¹C]FLB-457 values of the five thalamic subregions, dorsal anterior cingulate cortex (dACC), rostral anterior cingulate cortex (rACC), amygdala, ventral tegmental area, and substantia nigra. The closed and open circles represent individuals with ASD and TD individuals, respectively. Error bars represent standard errors.

Figure 2. Correlations between [^{11}C]FLB-457 binding potential (BP$_{ND}$) values in the posterior subregion of the thalamus and social affect (SA)-revised scores of the Autism Diagnostic Observation Schedule Second Edition (ADOS-2) in individuals with autism spectrum disorder (ASD)

Scatterplots show correlations between [^{11}C]FLB-457 BP$_{ND}$ values in the posterior subregion of the thalamus and SA-revised scores in individuals with ASD.

Figure 3. Results of the multivariate pattern analysis (MVPA) of resting-state functional

MRI data

(A) Thalamic (top) and right cerebellar (bottom) seeds identified by MVPA. These two

clusters showed significant group differences in the association between whole-brain

functional connectivity patterns and dopamine D2/3 receptor (D2/3R) availability averaged

across regions of interest. Numbers in parentheses indicate peak coordinates. (B) Results of

the post hoc seed-to-voxel analysis. The thalamus seed analysis revealed the bilateral superior

temporal sulcus (upper two rows; peak coordinate = [−56, −48, 10], cluster size = 1283, $t =$

5.83 for the left temporal cluster; peak coordinate = [50, 10, −34], cluster size = 1417, $t = 5.53$

for the right temporal cluster), whereas the right cerebellar seed revealed the right postcentral

gyrus and the medial occipital cortex, including the lingual gyrus and cuneus (lower two

rows; peak coordinate = [18, −52, −6], cluster size = 9495, $t = 8.20$ for the medial occipital

cluster; peak coordinate = [44, −18, 50], cluster size = 219, $t = 4.23$ for the right postcentral

cluster).

Table 1. Demographic characteristics of participants

Characteristics	Individuals with ASD (N = 22)		TD individuals (N = 24)			
	Mean	SD	Mean	SD	t value	p value
Age, years old	24.8	5.9	24.3	6.1	0.23	0.82
Height, cm	168.7	5.6	170.6	5.3	-1.15	0.26
Body mass index, kg/m^2	23.6	4.9	21.5	2.1	1.93	0.064
SES*	3.6	1.1	2.4	0.6	4.67	< 0.001
Parental SES*	2.5	1.0	2.5	0.8	0.01	0.99
Intelligence Quotient						
Full scale IQ	105.2	16.5	106.6	14.8	-0.30	0.76
Verbal IQ	108.9	16.3	108.0	14.6	0.19	0.85
Performance IQ	99.5	17.3	103.3	14.9	-0.81	0.42
Autism Spectrum Quotient	30.4	7.2	17.2	7.2	6.33	< 0.001
ADOS-2						
Reciprocity	7.0	1.6	NA			
Communication	3.1	1.4	NA			
RRB	1.5	1.4	NA			
Social Affect-revised	9.8	2.3	NA			
ADI-R						
Reciprocity	17.6	8.1	NA			
Communication	12.8	5.5	NA			
RRB	4.4	2.9	NA			

Abbreviations: ASD, autism spectrum disorder; TD, typically developing; IQ, intelligence quotient; ADOS-2, Autism Diagnostic Observation Schedule Second Edition; RRB, restricted and repetitive behaviors; ADI-R, Autism Diagnostic Interview-Revised; NA, not applied; SD, standard deviation; SES, socioeconomic status

*Assessed by the Hollingshead index; higher scores indicate lower status.

Table 2. [^{11}C]FLB457 binding potential (BP$_{ND}$) values in extrastriatal regions in ASD and TD individuals

Brain region	Individuals with ASD		TD individuals		*t* value	*p* value	Cohen's d
	Mean	SD	Mean	SD			
Substantia nigra	1.60	0.41	1.77	0.47	-1.30	0.20	0.38
VTA	1.46	0.53	1.51	0.41	-0.37	0.71	0.11
Amygdala	1.87	0.40	2.11	0.34	-2.19	0.034	0.65
Dorsal ACC	0.53	0.14	0.60	0.14	-1.78	0.082	0.53
Rostral ACC	0.40	0.16	0.43	0.12	-0.81	0.38	0.26
Thalamic subregion							
Anterior medial	1.77	0.41	2.01	0.42	-2.01	0.050	0.59
Anterior lateral	1.02	0.38	1.17	0.43	-1.26	0.21	0.37
Central medial	2.00	0.53	2.20	0.35	-1.55	0.13	0.46
Central lateral	1.09	0.24	1.26	0.30	-2.05	0.046	0.61
Posterior	1.17	0.26	1.43	0.29	-3.23	0.0023	0.95

Abbreviations: ASD, autism spectrum disorder; TD, typically developing; VTA, ventral tegmental area; ACC, anterior cingulate cortex; SD, standard deviation
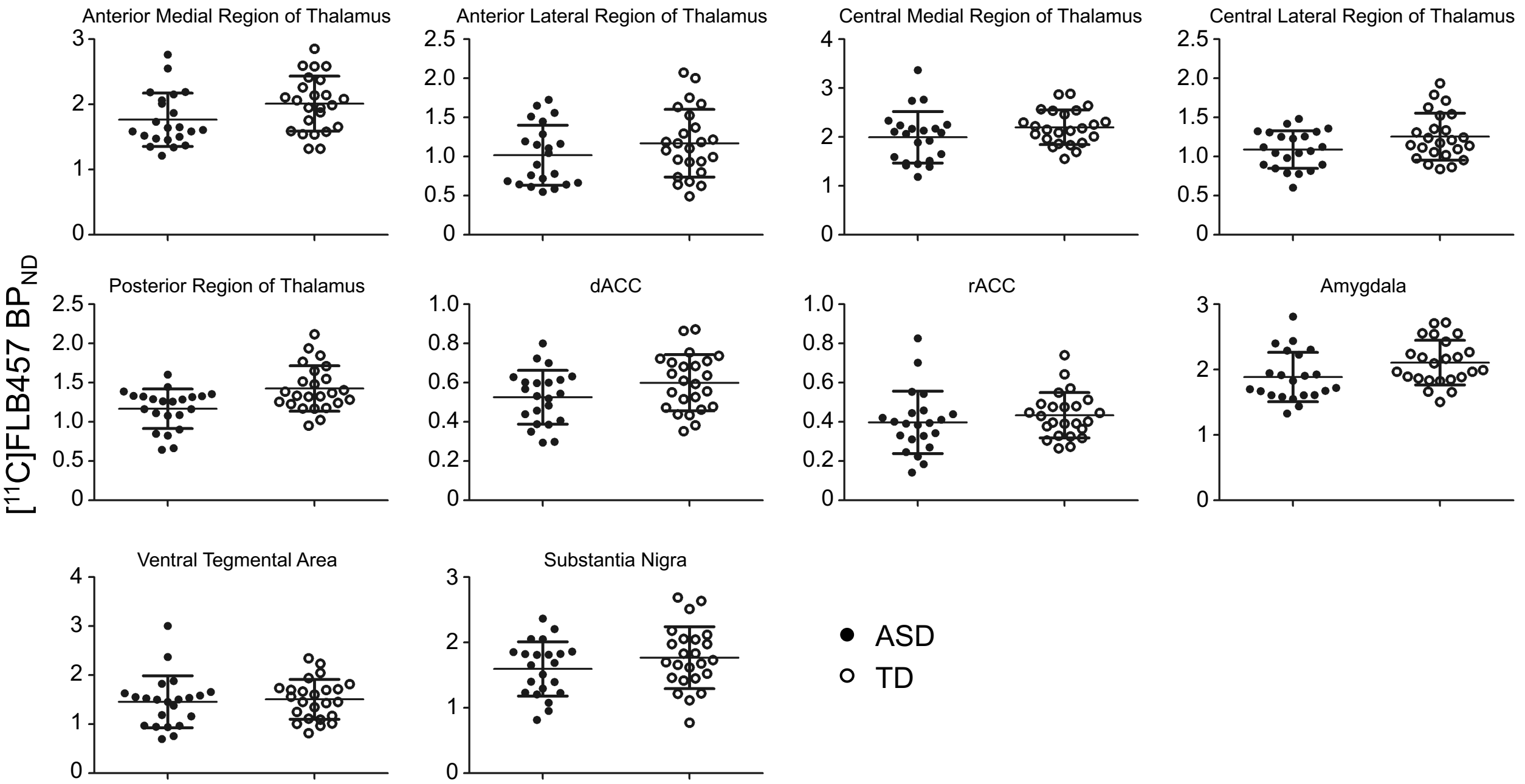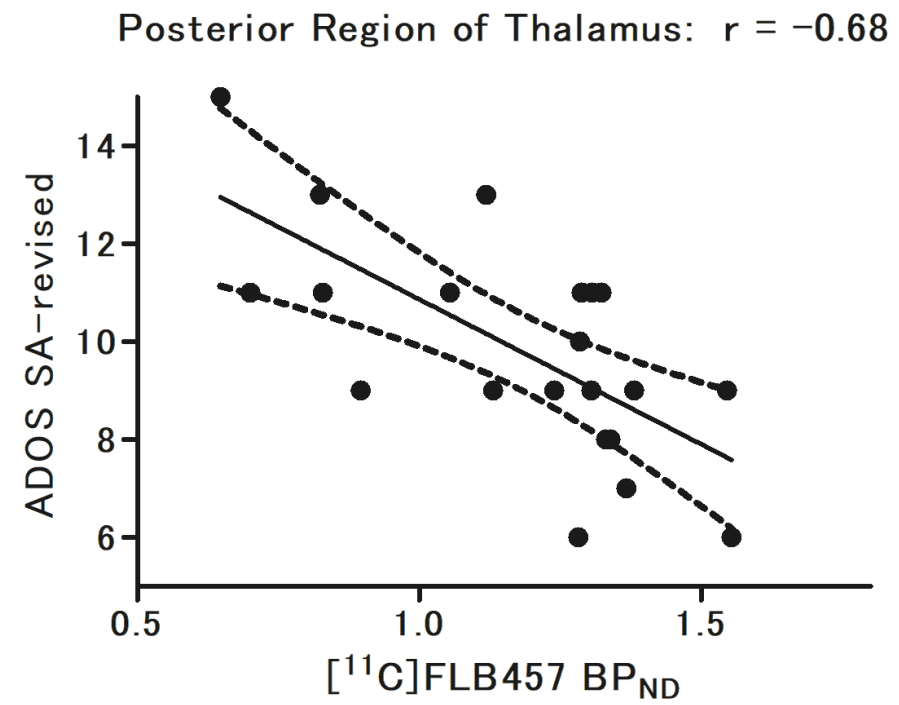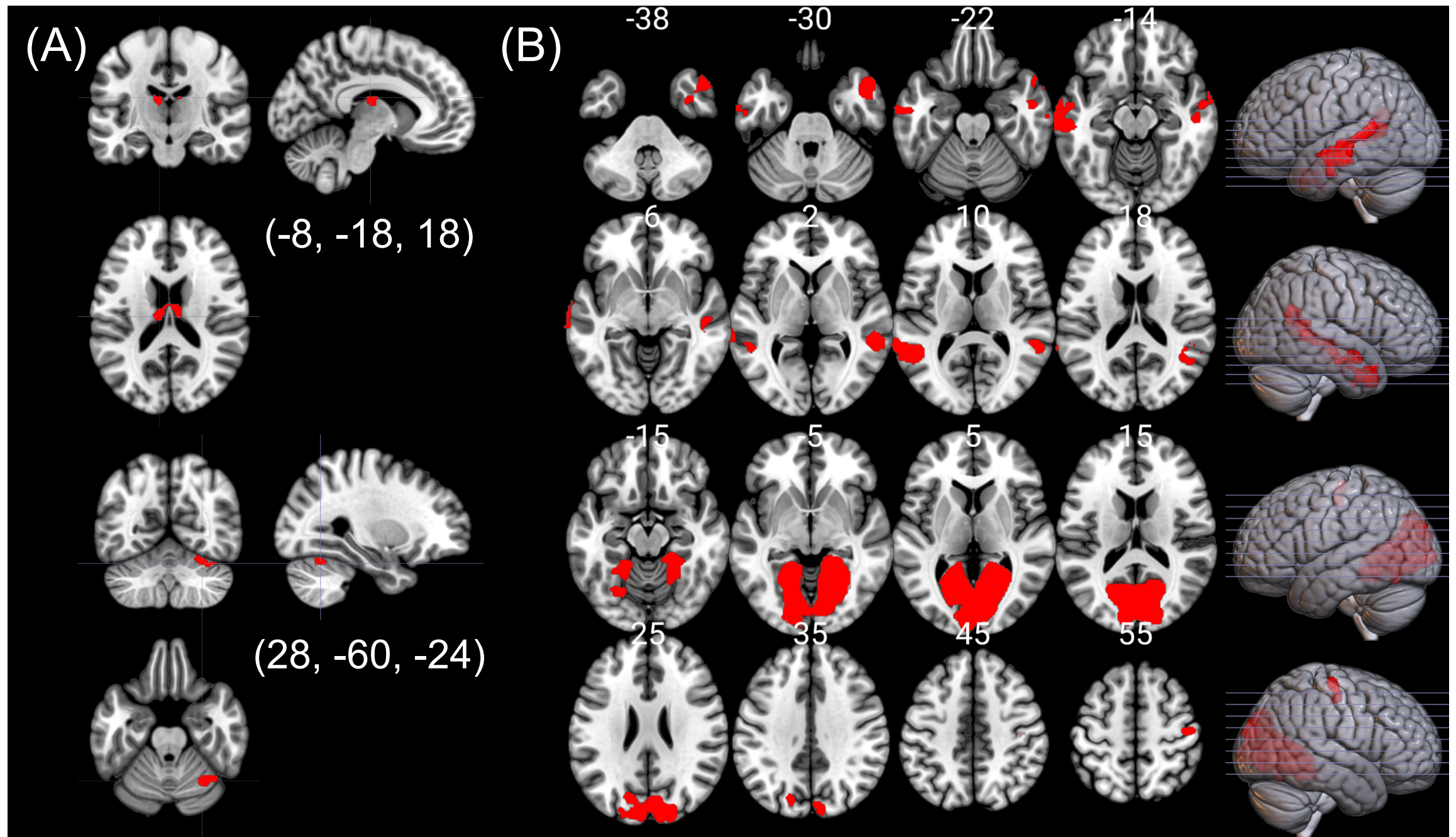
Figure 1

Figure 2

Posterior Region of Thalamus: r = −0.68

Figure 3

(A)

(-8, -18, 18)

(28, -60, -24)

(B)

-38   -30   -22   -14

6   2   10   18

-15   5   5   15

25   35   45   55

Supplementary information for
Murayama et al., "Extrastriatal dopamine D2/3 receptor binding, functional connectivity, and autism socio-communicational deficits: a PET and fMRI study"

Supplementary Methods

Supplementary References

Supplementary Figure 1. Examples of regions of interest and reference cerebellar cortex

Supplementary Figure 2. Thalamic subdivisional regions of interest

Supplementary Figure 3. The subdivisional regions of interest in anterior cingulate cortex

Supplementary Figure 4. Representative [^{11}C]FLB-457 binding potential (BP$_{ND}$) PET images

Supplementary Figure 5. Correlations between [^{11}C]FLB-457 binding potential (BP$_{ND}$) values in the posterior subregion of the thalamus and the three domain scores of the Autism Diagnostic Observation Schedule Second Edition (ADOS-2) in individuals with ASD

Supplementary Figure 6. Correlations between [^{11}C]FLB-457 binding potential (BP$_{ND}$) values averaged across regions of interest and resting-state functional connectivity

Supplementary Table 1. Correlations between ADOS scores and functional connectivity revealed by the post hoc analysis

Supplementary Methods

Division of the anterior cingulate cortices (ACC) and thalamus for ROI analysis

The anatomical border between the dACC and rACC was defined on the coronal plane that was one slice anterior to the disappearance of the juncture of the anterior corpus callosum of both hemispheres (1, 2). The posterior border of the dACC was the first vertical slice posterior to the anterior commissure (1).

The thalamus was first divided into medial and lateral parts. The vertical bisection (coronal view of Supplementary Figure 2) was accomplished by a bisector drawn parallel to the lateral border of the midbrain, the interhemispheric fissure, and the cerebral aqueduct. This bisector continued through all thalamic slices to create a plane of bisection parallel to the interhemispheric fissure. We then measured contiguous coronal slices of the thalamus and divided the thalamus into anterior, central, and posterior divisions. The anterior and central divisions each contained 40% of the total number of slices; the posterior division contained 20% of the total number of slices (axial and sagittal views of Supplementary Figure 2). Using this approach, the thalamus was divided into six subregions. The medial and lateral portions of the posterior thalamus were combined because they both corresponded to the pulvinar. This resulted in five thalamic subregions:

the anterior medial, anterior lateral, central medial, central lateral, and posterior

subregions (axial view of Supplementary Figure 2).

MRI data acquisition and resting-state fMRI data preprocessing

To normalize functional data and establish ROIs, T1-weighted images were collected with

the following parameters: repetition time (TR) = 6.8 ms, echo time (TE) = 3.1 ms, flip

angle = 9°, voxel size = $1.0 \times 1.0 \times 1.2$ mm^3 with slice thickness of 1.2 mm, matrix = 256

$\times$ 256, and 170 sagittal slices. A mobile PET gantry allowed us to reconstruct the PET

images parallel to the AC-PC line without reslicing. For resting state functional imaging,

T2*-weighted gradient-echo echo-planner images were also acquired with the following

parameters: TR = 3000 ms, TE = 30 ms, flip angle = 90°, slice thickness = 3.4 mm, voxel

size = $3.4 \times 3.4 \times 3.4$ mm^3, matrix = 64×64, 48 transversal slices with an interleaved

slice order (the default of the Philips scanner), and 197 volumes with four dummy scans.

Participants were instructed to gaze at a black fixation cross on a light gray background

through an MRI-compatible head-mounted display (Visual Stim Digital; Resonance

Technology Company, Inc., Los Angeles, USA) during a 10-min resting-state fMRI run.

After the first four volumes were discarded to avoid T1 equilibrium effects, remaining

functional data (i.e., 193 volumes) were realigned, corrected for slice timing, spatially

normalized to Montreal Neurological Institute space, and smoothed with an 8-mm full-width half-maximum kernel. Using the denoising pipeline implemented in the CONN toolbox, we conducted temporal band-pass filtering (0.008–0.09 Hz). To remove physiological and motion-related artifacts, we regressed out signals from white matter and cerebrospinal fluid as well as motion outliers (with a volume-to-volume threshold of 0.9 mm and a global mean intensity threshold of 5 standard deviations) and Friston 24 head-motion parameters (3). Three ASD participants with fewer than 155 eligible volumes (i.e., < 80% of the total volumes) were excluded from subsequent analyses because of excessive motion-related outliers. For the remaining participants (19 ASD and 24 TD), we found no significant differences in mean frame-wise motion ($t = 0.8$, $p = 0.5$) or number of ineligible volumes ($t = 0.5$, $p = 0.6$) between groups.

Statistical analysis for resting-state fMRI data: Multivariate pattern analysis (MVPA)

MVPA, which is implemented in the CONN toolbox, is a well-validated data-driven method that was developed to unbiasedly identify seed regions for seed-to-voxel functional connectivity analysis (4, 5). Our MVPA aimed to explore regions where whole-brain functional connectivity showed a significant interaction between D2/3R

availability and diagnosis. For the variable of D2/3R availability, we used [^{11}C]FLB457

BP$_{ND}$ values averaged across the ROIs that exhibited significant differences between

ASD and TD groups. Using the MVPA pipeline in the CONN toolbox, multivariate

functional connectivity patterns from each voxel to the rest of the brain were computed.

Then, using principal component analysis, the dimensionality of this multivariate

functional connectivity was reduced to 64 spatial components. The first three

components were retained to create MVPA maps for the group-level analysis. We

considered the number of retained components adequate because the top three

components explained 80% and 88% of the variance for white and gray matter,
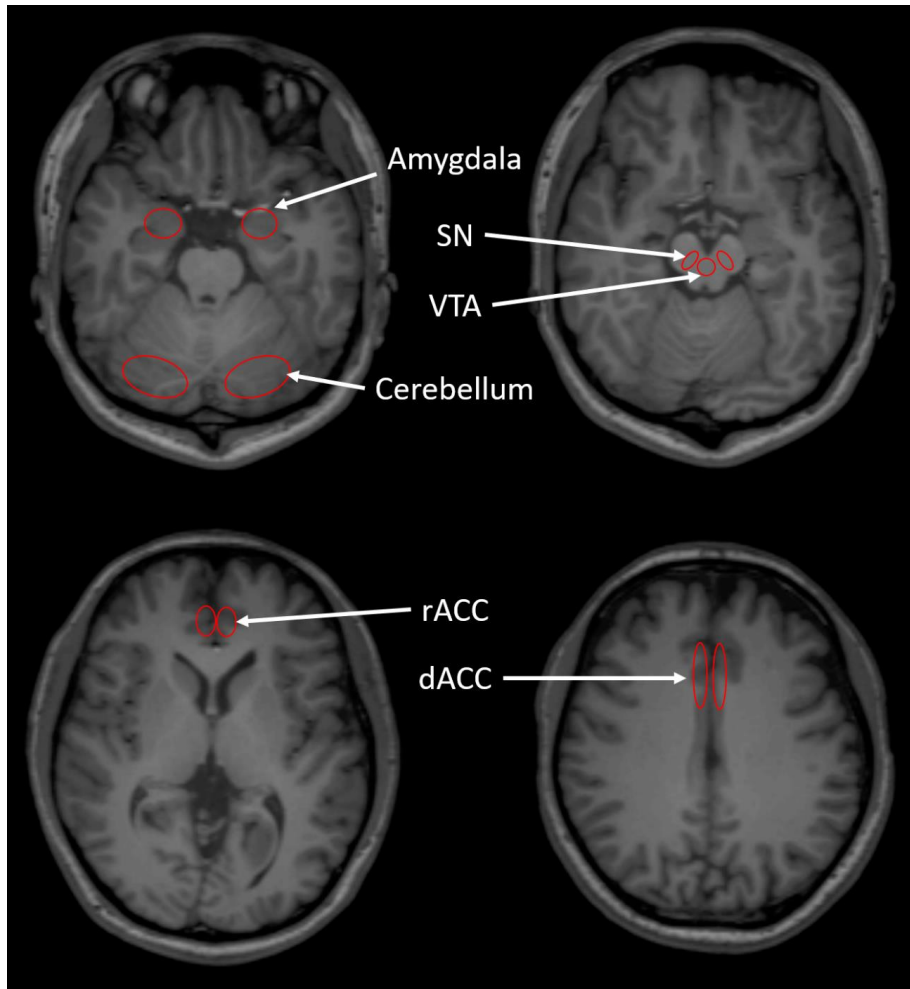
respectively (5).

Using the MVPA-derived maps as the dependent variables, we conducted a

multivariate analysis of covariance (MANCOVA). Four independent variables were

included in the MANCOVA: two group variables (one coded as 1 = ASD, 0 = TD; the

other coded as 1 = TD, 0 = ASD) and two continuous variables of D2/3R availability

(one coded as individual values of the averaged [^{11}C]FLB457 BP$_{ND}$ for ASD and 0 for

TD; the other coded vice versa). We explored regions where whole-brain functional

connectivity patterns were differentially associated with [^{11}C]FLB457 BP$_{ND}$ values

between groups by specifying the contrast [0 0 1 −1] for the four independent variables.

The statistical map, exclusively masked by gray matter structures, was initially

thresholded at the voxel level of $p < 0.001$ (uncorrected, two-tailed) and subsequently at

the cluster level of $p < 0.05$ (family-wise error corrected for multiple comparisons). The

same thresholding was used for the post hoc seed-to-voxel analysis.
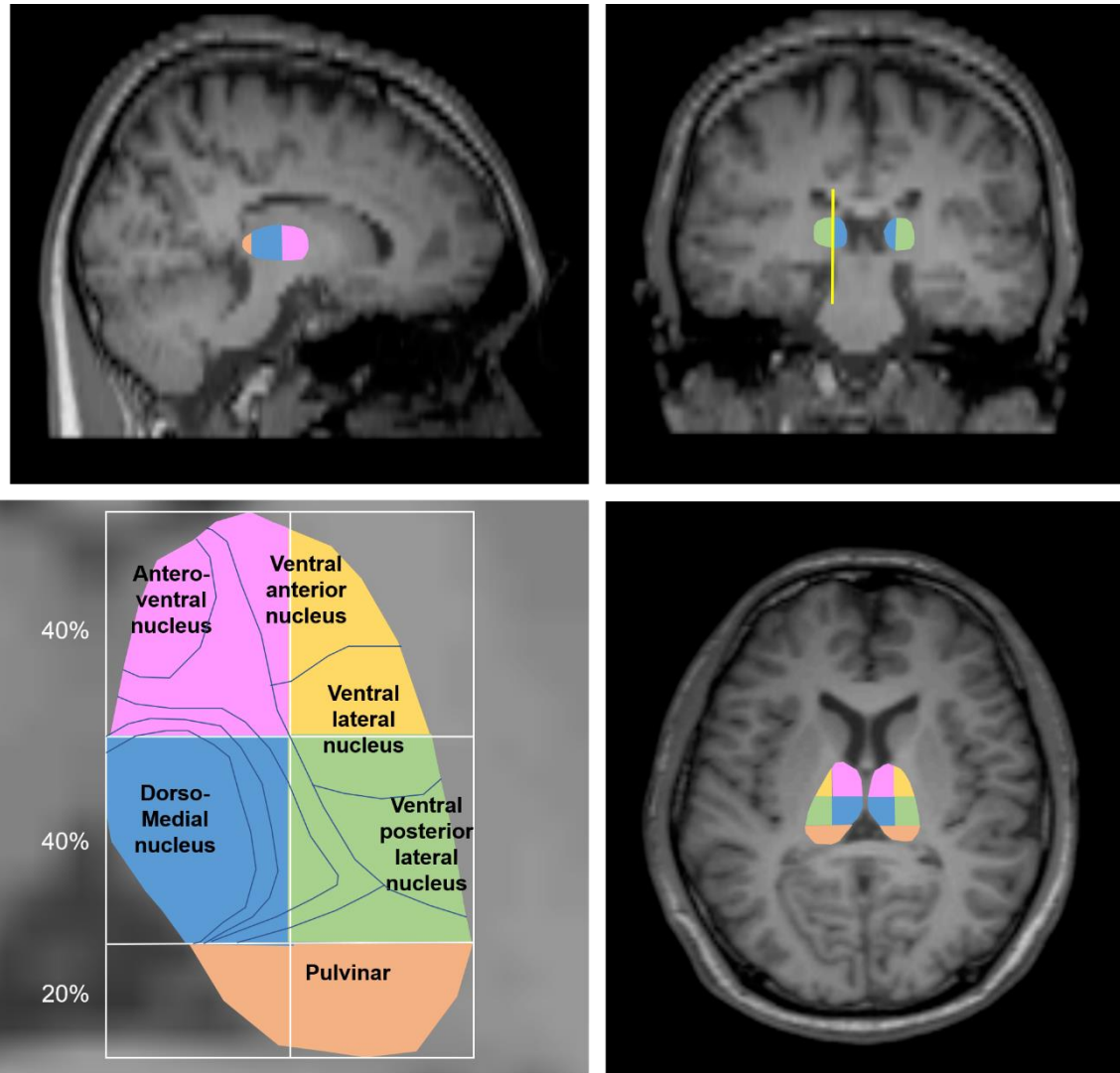
Supplementary References

1. Fornito A, Whittle S, Wood SJ, Velakoulis D, Pantelis C, Yücel M. The influence of sulcal variability on morphometry of the human anterior cingulate and paracingulate cortex. *Neuroimage*. 2006;**33**(3):843-54.

2. McCormick LM, Ziebell S, Nopoulos P, Cassell M, Andreasen NC, Brumm M. Anterior cingulate cortex: an MRI-based parcellation method. *Neuroimage*. 2006;**32**(3):1167-75.

3. Friston KJ, Williams S, Howard R, Frackowiak RS, Turner R. Movement-related effects in fMRI time-series. *Magn Reson Med*. 1996;**35**(3):346-55.

4. Whitfield-Gabrieli S, Ghosh SS, Nieto-Castanon A, Saygin Z, Doehrmann O, Chai XJ, et al. Brain connectomics predict response to treatment in social anxiety disorder. *Mol Psychiatry*. 2016;**21**(5):680-5.

5. Wang Y, Bernanke J, Peterson BS, McGrath P, Stewart J, Chen Y, et al. The association between antidepressant treatment and brain connectivity in two double-blind, placebo-controlled clinical trials: a treatment mechanism study. *The Lancet Psychiatry*. 2019;**6**(8):667-74.

6. Yasuno F, Suhara T, Okubo Y, Sudo Y, Inoue M, Ichimiya T, et al. Low dopamine d(2) receptor binding in subregions of the thalamus in schizophrenia. *Am J Psychiatry*. 2004;**161**(6):1016-22.

7. Gilbert AR, Rosenberg DR, Harenski K, Spencer S, Sweeney JA, Keshavan MS. Thalamic volumes in patients with first-episode schizophrenia. *Am J Psychiatry*. 2001;**158**(4):618-24.

Supplementary Figure 1. Examples of regions of interest and reference cerebellar cortex
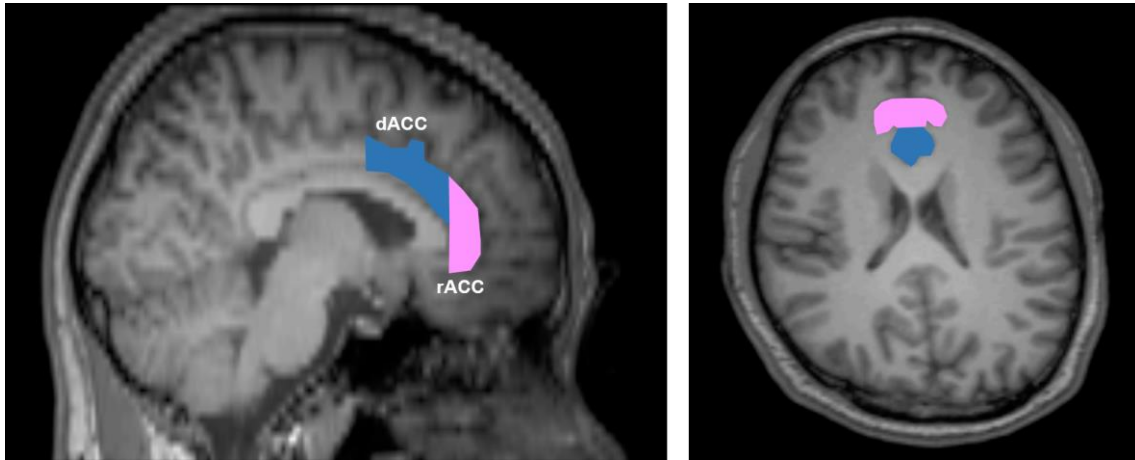

Abbreviations: SN, substantia nigra; VTA, ventral tegmental area; rACC, rostral anterior cingulate cortex; dACC, dorsal anterior cingulate cortex

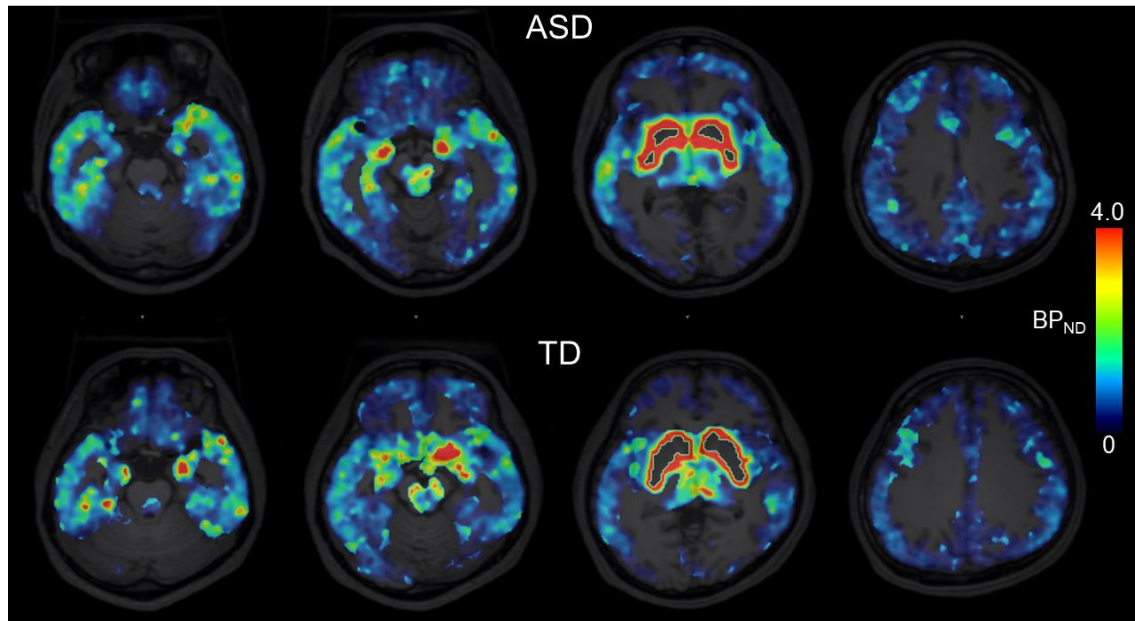**Supplementary Figure 2. Thalamic subdivisional regions of interest**

In the axial view of the thalamus (lower left), approximate regions of specific thalamic nuclei are described with reference to previous articles (6, 7). In the coronal view, the line represents a vertical bisector, which was drawn parallel to the lateral border of the midbrain, interhemispheric fissure, and cerebral aqueduct.

Supplementary Figure 3. The subdivisional regions of interest in anterior cingulate cortex
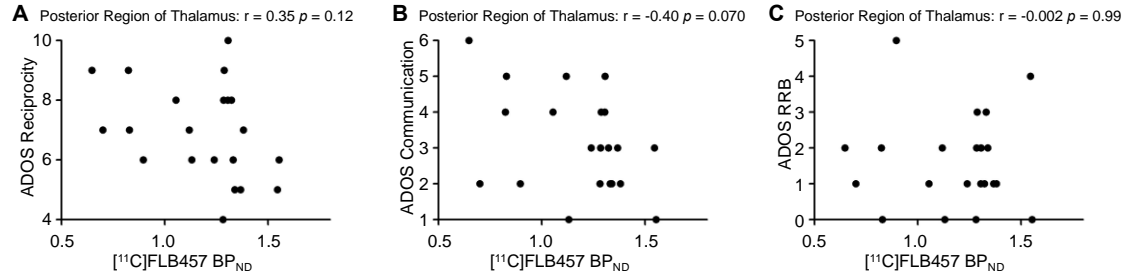

In the sagittal (left) and axial view (right), approximate locations of subdivisions of anterior cingulate cortex (ACC) including dorsal ACC (dACC in blue) and rostral ACC (rACC in pink) are presented.

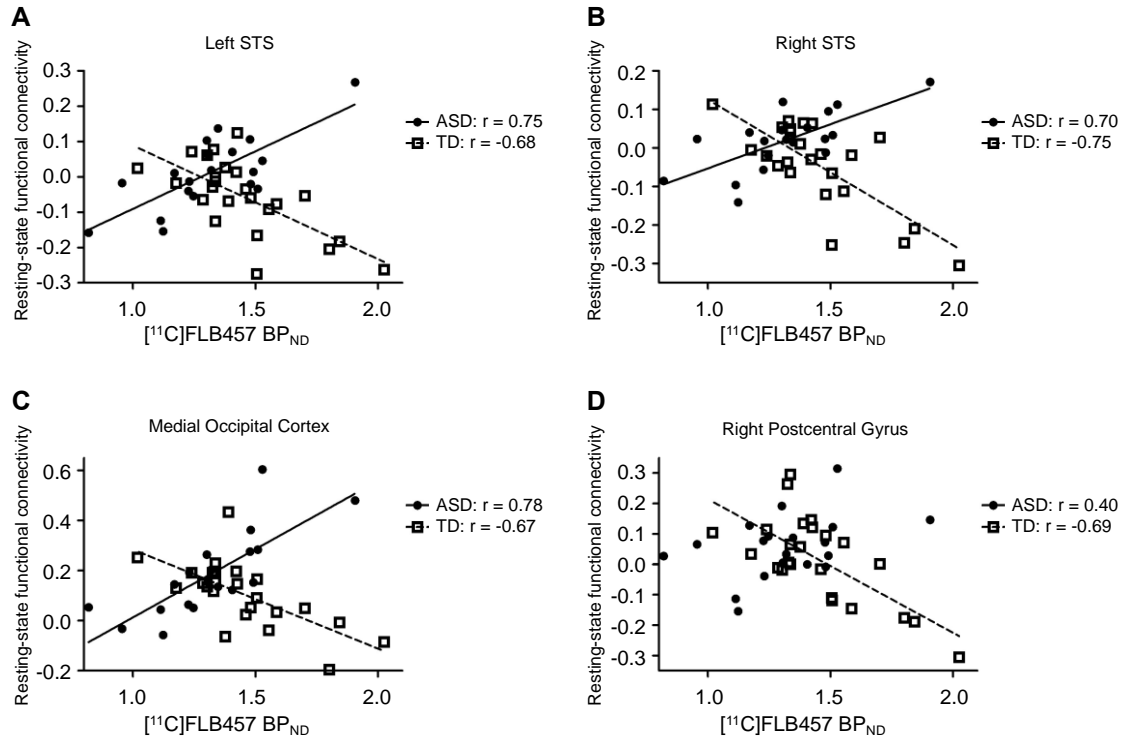**Supplementary Figure 4. Representative [¹¹C]FLB-457 binding potential (BP$_{ND}$) PET images**

Representative [¹¹C]FLB-457 PET images of ASD and TD individuals. Abbreviations: ASD, autism spectrum disorder; TD, typically developing

Supplementary Figure 5. Correlations between [^{11}C]FLB-457 binding potential (BP$_{ND}$) values in the posterior subregion of the thalamus and the three domain scores of the Autism Diagnostic Observation Schedule Second Edition (ADOS-2) in individuals with ASD

Scatterplots show correlations between [^{11}C]FLB-457 BP$_{ND}$ values in the posterior subregion of the thalamus and scores on reciprocity (**A**), communication (**B**), and restricted and repetitive behaviors (RRB) (**C**).

Supplementary Figure 6. Correlations between [^{11}C]FLB-457 binding potential (BP$_{ND}$) values averaged across regions of interest and resting-state functional connectivity

Scatterplots show correlations between [^{11}C]FLB-457 BP$_{ND}$ values and functional connectivity of the thalamus–left superior temporal sulcus (STS) (A), thalamus–right STS (B), right cerebellum–medial occipital cortex (C), and right cerebellum–right postcentral gyrus (D). Closed circles and open squares represent ASD and TD individuals, respectively.

Supplementary Table 1. Correlations between ADOS scores and functional connectivity revealed by the post hoc analysis

	Reciprocity		Communication		RRB		SA-revised	
	r	*p*	*r*	*p*	*r*	*p*	*r*	*p*
Thalamus seed								
L Superior temporal gyrus	-0.21	0.41	0.09	0.74	0.05	0.83	-0.13	0.61
R Superior temporal gyrus	-0.09	0.71	0.05	0.84	0.21	0.41	-0.16	0.53
Cerebellum seed								
R/L Medial occipital cortex	-0.12	0.64	-0.03	0.92	0.01	0.96	-0.14	0.59
R Postcentral gyrus	0.331	0.18	0.29	0.24	0.20	0.43	0.34	0.16

Pearson's correlation coefficients and uncorrected *p*-values are shown. Abbreviations: L, left; R, right; RRB, restricted and repetitive behaviors; SA-revised, social affect-revised; RRB-revised, restricted and repetitive behaviors-revised.